

Solar-induced fluorescence (SIF) of C₂ radical

J.M. Badie^a, G. Flamant^{a,*}, T. Guillard^a, D. Laplaze^b

^a Institut de Science et de Génie des Matériaux et Procédés, IMP-CNRS, B.P. 5, Odeillo, 66125 Font-Romeu Cedex, France

^b Groupe de Dynamique des Phases Condensées, UM2-CNRS, c.c. 026, Université de Montpellier II, Place E. Bataillon, 34095 Montpellier Cedex, France

Received 17 October 2001; in final form 11 March 2002

Abstract

C₂ Swan band emission ($d^3\pi_g \rightarrow a^3\pi_u$) near 517 nm is observed in a solar reactor for fullerene synthesis. On the basis of theoretical considerations and experimental results in the temperature range 3000–3400 K evidence is presented supporting the formation of excited C₂ by absorption of solar photons. This phenomenon that we propose to name: solar-induced fluorescence (SIF) is described for the first time. © 2002 Elsevier Science B.V. All rights reserved.

1. Introduction

Three high temperature methods can produce fullerenes and single-wall nanotubes (SWNTs); there are namely the laser ablation, the electric arc and the solar methods. Laser-generated vapors produced fullerenes for the first time in 1985 [1]. Then Krütschmer et al. [2] succeeded in producing milligram amounts of fullerenes by the arc method (resistive heating of graphite in a helium atmosphere). The solar method was developed at the same time (1993) in USA [3,4] in France [5], and we successfully proposed an extrapolation method, which permitted, at a first step, to produce 1 g/h fullerene by solar energy [6]. Next, we have extended the solar method to the synthesis of SWNTs [7]. Whatever the method, the understanding of formation mechanisms involves two

basic questions: What are the precursors of the molecules (C₆₀) or the material (SWNTs)? And what is the temperature history of the species that favours the product growth?

The detection of species (atoms, molecules, ions and clusters) produced by laser ablation has received a great attention from many researches [8–10] (and permits fullerene discovery). They used generally photoionization/mass spectroscopy, optical emission spectroscopy (OES) and laser-induced fluorescence (LIF). More recently, Lange et al. [11] and Arepalli et al. [12] used OES and LIF in order to determine temperatures in fullerene and nanotubes arc plasma and pulsed laser reactors, respectively. In any case, C₂ radical is detected and may be used as a temperature probe. For that purpose, emission of the Swan band ($d^3\pi_g, v' = 0 \rightarrow a^3\pi_u, v'' = 0$) in the wavelengths range 436–668 nm permits to define a rotational temperature of the gas. We performed OES measurements of C₂ emission using our solar reactor and, surprisingly, we observed intense rotational band in the

* Corresponding author. Fax: +33-4-68-30-2940.

E-mail address: flamant@imp.cnrs.fr (G. Flamant).

target temperature range 3000–3500 K. This observation addresses another question: What is the excitation mechanism of C_2 in the solar reactor?

Excitation mechanisms of C_2 causing Swan band emission are discussed in [8,10,12,13], for example. They can be classified in five processes: (1) direct excitation by electron collisions; (2) low-energy electron collisions with C_n cations ($n \geq 2$) and neutrals ($n > 2$) followed by dissociation; (3) heavy-body collisions of the second kind such as Penning collisions with atomic or molecular metastable states; (4) recombination mechanisms: slow electron processes: electron-molecule dissociative attachment, electron-ion and ion-ion recombination; or chemiluminescence (recombination of carbon atoms); (5) photon processes:

photodissociation of carbon clusters or fluorescence of C_2 . Among these excitation mechanisms we show in this paper that solar-induced fluorescence of C_2 is the most probable. From our knowledge, this phenomenon is reported for the first time.

2. Experimental

A schematic of the experimental system is given in Fig. 1. It was previously described in [14]. Two main subsystems can be considered: (1) the reactor and the solar concentrator, (2) the measurement equipments composed of a pyrometer and an optical emission spectrometer.

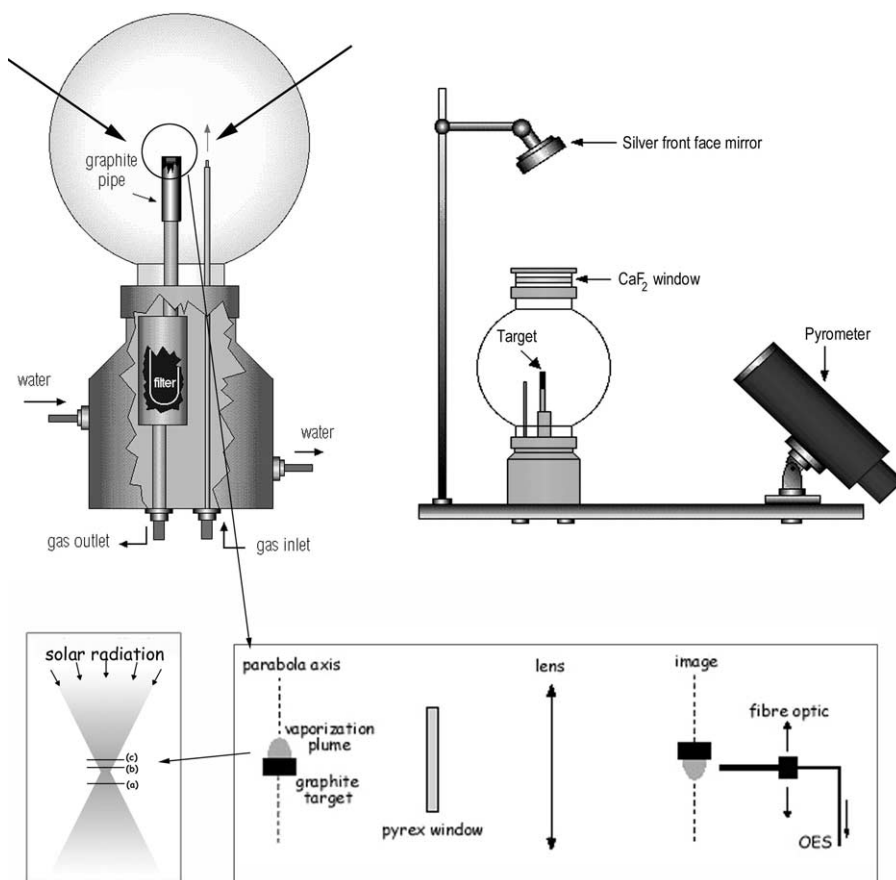


Fig. 1. Experimental apparatus. The reactor (top left), the pyrometer assembly (top right), the OES system (bottom right) and the target position with respect to the solar furnace focus during experiment 1 (bottom left).

2.1. Reactor and solar concentrator

The vaporization of the graphite target was performed in spherical transparent vessel (pyrex), which permitted the target heating by concentrated solar energy and the control of reacting atmosphere composition and pressure. The base of the reactor was a water-cooled brass stand part equipped with a cellulose filter for soot collection. The filter was connected to a copper tube channelling the argon–soot mixture from the vaporization zone. The upper part of the tube was made of graphite due to high temperature in the hot zone. The target, a 7.7 mm o.d. and 7.7 mm by graphite rod was inserted in the graphite tube (10.5 mm i.d.). A stainless steel tube located near the target allowed the buffer gas (argon) injection. Then it flowed through the empty space between the target and the graphite tube, pumped by the circulation equipment composed of a vacuum pump and a pressure regulator.

The graphite target was heated by concentrated solar energy delivered by a vertical axis 2 kW-solar furnace (a parabolic reflector concentrating the solar beams reflected a flat mirror tracking the sun). The flux density distribution at the focus of the solar furnace was gaussian with a peak at about 1600 W/cm^2 (16 MW/m^2). Moving the target surface vertically along the z -axis (furnace axis) resulted in a drastic decrease of the peak flux density because of the wide optical aperture of the parabola (120°). The peak flux density was varied slightly near the focus: about 5% decrease for a $\pm 2 \text{ mm}$ vertical movement but it decreases rapidly for larger displacement: about 2 MW/m^2 decrease per mm for $|z| > 3 \text{ mm}$.

2.2. Measurement equipments

We measured the target surface temperature with an IR pyrometer and the emission of the evaporation plume by OES (see Fig. 1).

The optics of the pyrometer (Heymann apparatus) sighted the target surface through a CaF_2 window thanks to a silver mirror placed on the axis of the reactor (axis of the parabola). We made monochromatic measurement at $\lambda = 2.7 \mu\text{m}$. At this wavelength the contribution of reflected solar

energy may be neglected because it corresponds to the centre of an OH absorption band. Nevertheless, the target spectral emissivity (ε_λ) is needed to define the true surface temperature. Neuer [15] showed that ε_λ decreases with wavelength and increases with temperature. In the temperature range 3000–3500 K we assumed $\varepsilon_\lambda = 0.95$ ($\lambda = 2.7 \mu\text{m}$). Five percent uncertainty on ε_λ ($\varepsilon_\lambda = 0.95 \pm 0.05$) corresponds to $\pm 100 \text{ K}$ at this temperature level.

The optical emission spectrometry set up is schemed in Fig. 1. An optical port (not shown in Fig. 1) allowed sighting the vaporization plume above the target perpendicularly to the parabola axis (tangentially to the target surface). A lens (focal distance 300 mm) made the plume image at one end of a fibre optic mounted on a z - r displacement device. The other end of the $100 \mu\text{m}$ core diameter fibre optic was connected to the monochromator. Since the magnification of the optics was unity; the spatial resolution of the measurement was $100 \mu\text{m}$. The monochromator (Jobin Yvon Triax 320) was equipped with three diffraction gratings: 300, 1200 and 1800 lines/mm. We have used the medium grating with a $50 \mu\text{m}$ inlet slot. The detector was the CCD matrix (1024×128 pixels) of a multichannel optical analyser (MOA). The spectral width of each photodiode was about 0.1 nm and the spectral domain extent was 70 nm centred at the selected wavelength.

3. Results

We have performed experiments with argon as buffer gas in the pressure and the gas flow rate ranges 70–400 hPa and 0.1–1 Nm^3/h , respectively, with target made of either graphite rods or compressed graphite powder pellets. Measured surface temperature was ranging from 3000 to 3500 K and 3000 to 3700 K for rod and compressed powder, respectively. The corresponding vaporization rate was $0.4\text{--}40 \text{ g s}^{-1} \text{ m}^{-2}$. We have observed a vaporization plume in the whole range of pressure, but it was more stable at low pressure and low gas flow rate than at pressure of some hundreds hPa due to convective instability in this latter case. The Swan band emission was very intense close to the target surface at temperatures as low as 3000 K. It

can be used to measure the rotational temperature of C_2 [16] down to 2300 K at distances up to 1.6 mm from the surface. Surprisingly it remains very clearly observable at distances from the surface up to 2.5 mm where the gas temperature is expected to be at about 2100 K from simulation [14]. We assumed that SIF of C_2 might be the cause of this observation involving an absorption process similarly to LIF. In order to check this assumption, we have performed both a quantitative theoretical estimation of C_2 emission contributions and an experimental validation.

3.1. Quantification of the emission

The idea that fluorescence induced by solar photons is the main mechanism of C_2 emission is supported by the following considerations. Let us consider that the levels population density follow a Boltzman statistic, the line thermal emission intensity at λ for a given sampled volume V and the transition $2 \rightarrow 1$ is

$$L_\lambda = \frac{\Omega}{4\pi} V \frac{hc}{\lambda} \frac{N_0(T)}{Q(T)} g_2 A_{21} \exp\left(-\frac{E_2}{kT}\right), \quad (1)$$

where Ω is the insight solid angle, N_0 is the fundamental level population density, $Q(T)$ is the partition function of the considered species and g_2 and E_2 are the degeneracy and the energy level of the upper emission level, respectively. The other symbols have their usual significance.

For this same volume, the fluorescence intensity is given by [17]

$$F_\lambda = \frac{\Omega}{4\pi} V \frac{\lambda^4}{8\pi c} \frac{N_0(T)}{Q(T)} g_2 A_{21} I_\lambda \Phi_{21}, \quad (2)$$

where I_λ is the solar spectral irradiance.

In Eq. (2), the classical relation between absorption (B_{12}) and emission (A_{21}) Einstein coefficients is used in order to exhibit the ratio between fluorescence and thermal emission

$$\frac{F_\lambda}{L_\lambda} = \frac{\lambda^5}{hc^2} \frac{I_\lambda \Phi_{21}}{8\pi} \exp\left(\frac{E_2}{kT}\right). \quad (3)$$

The term $\Phi_{21} = A_{21}/(A_{21} + Q_{21})$ is the fluorescence efficiency where Q_{21} represents the collisional quenching rate for the excited state.

To the best of our knowledge there is no measured data about the quenching rate of C_2 $d^3\Pi_g$ by argon. Nevertheless, argon belongs to a class of species that have a negligible quenching cross section according to the attractive force model of Paul [18], i.e., less than 10^{-21} m² as for OH $A^2\Sigma^+$ or NO $A^2\Sigma^+$ [19]. Assuming the same value for the quenching cross section of C_2 $d^3\Pi_g$ by argon, this would lead to a quenching rate less than 4×10^5 s⁻¹ for our conditions. The emission coefficient being about 8.3×10^6 s⁻¹ for the C_2 observed transition, it comes that Φ_{21} is close to unity. On this basis, Table 1 lists the values of the ratio F_λ/L_λ as a function of the distance z from the focal plane. The related gas temperature is obtained from the numerical simulation proposed in [14]. This estimation takes into account the spatial decrease of the solar irradiance.

The data in Table 1 show that, in our conditions, the C_2 radiation could result mainly from fluorescence due to the irradiation of the vapors by the solar concentrated beam because, whatever the position, the ration between fluorescence and thermal emission is always larger than 3 and can reach more than 100 at low temperature.

3.2. Experimental validation

If C_2 fluorescence induced by concentrated solar energy is the main cause of intense Swan band emission; thus the phenomena must be more intense near the focal plane than some millimetres from the focus because the solar flux density decreases in these zones (above and underneath the focal plane). For that reason we have performed OES measurements for the three positions of the

Table 1
Temperature dependence of the ratio between fluorescence and thermal emission of C_2

z (mm)	T (K)	I_λ (10^{13} W/m ² m)	F_λ/L_λ
0	3300	2.15	3
0.5	3080	2.11	6
1	2840	2.08	13
1.5	2600	2.04	32
2	2400	2	80
2.5	2100	1.97	440

Table 2
Experimental results for solar-vaporized graphite target

Level	z_s (mm)	T_s (K)	z_{sv} (mm)	I (ua)	T_g (K)	$\Delta T = T_s - T_g$	N (10^{17} m^{-3})
a	-3	3000	-2.5	4700	2850	150	115
b	1	3300	1.5	10 400	2950	350	360
c	3	3000	3.5	150		> 350	< 9

target surface schemed in Fig. 1. Positions (a)–(c) were situated 3 mm underneath the focal plane ($z_s = -3$ mm), 1 mm above the focal plane ($z_s = +1$ mm) and 3 mm above the focal plane ($z_s = +3$ mm), respectively. The equilibrium temperature of the target surface (T_s) was the same at position (a) and position (c) because they were symmetrical with respect to the focal plane. It was measured $T_s = 3000$ K. Consequently, the vaporization rate was the same because, at a given pressure (70 hPa for this experiment), it is a function only of temperature; this means that carbon species density was the same at equilibrium.

Table 2 presents the experimental results obtained for different positions of the target surface with respect to the focal plane (z_s). The surface temperature (T_s) was measured as well as the peak intensity (I) of the (0, 0) band head at a distance z_{sv} from the focal plane. From the C_2 Swan band emission, collected in the sampled volume, we have determined the rotational temperature [16], which is assumed to be the gas temperature (T_g). Finally, N is the C_2 number density assuming LTE.

The measured emission spectra 0.5 mm above the surface (location z_{sv}) when the target is at positions (a) and (c) are plotted in Fig. 2. This plot clearly shows that C_2 emission is very intense when the target is at position (a) and, by contrast, emission is weakly detected when the target is at position (c). Consequently, at this latter position the gas temperature measurement was impossible. These results show that the vapors cooled differently according to the surface position with respect to the focal plane. Obviously, there is a noticeable interaction between the vapors and the solar beam whatever the position. On that account the variation of ΔT (difference between the surface temperature and the gas temperature) observed as a function of surface position can probably be ex-

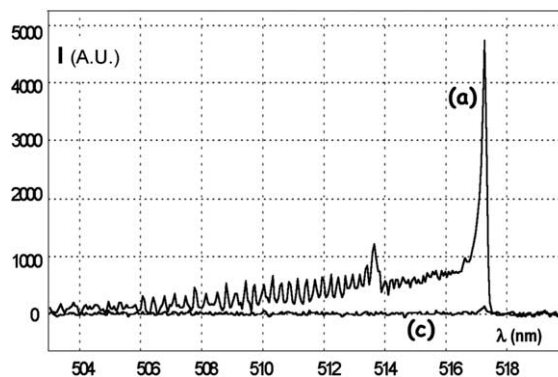


Fig. 2. Emission spectrum of C_2 in argon ($P = 70$ hPa) at position (a) and (c) – see Fig. 1 – for the same graphite target surface temperature (3000 K).

plained by the variation of solar irradiation. Below the focal plane (position (a)) the irradiation increases from the target to the focal plane, and the gas can absorb more and more energy from the solar beam as z increases. This process slows down the gas temperature decrease. On the contrary, when the surface is above the focal plane (positions (b) and (c)) the solar irradiation decreases with the distance z and, consequently, the gas temperature decreases more rapidly because the medium absorbs less and less solar radiation. These considerations can explain why ΔT is higher at position (c) than at position (a) despite the distance from the surface is the same. Elsewhere, condensation of the vapors can occur leading to a dilute dusty medium. Under the assumption of thermodynamic equilibrium between the vapor species and the particles resulting from the condensation, one can calculate a number density, N , of C_2 species (Table 2) from the measured temperature T_g . The same temperature difference, ΔT , is assumed for the positions (b) and (c) in order to estimate the density of species at (c), although it is

probably higher for this position due to a lower irradiation.

Generally speaking the fluorescence intensity is proportional to the species density (N) and the spectral irradiation (I_λ) as shown in Eq. (2). In this regard, the C_2 emission intensity must be higher at position (a) than at position (c) because both parameters N and I_λ are larger in (a) than in (c). According to the data listed in Table 2, the value of the ratio between C_2 emission peak intensity related to (a) and (c) is theoretically 15 and the measured value is about 30, which is a satisfactory agreement.

Let us now compare the C_2 emission for positions (a) and (b). The solar flux density was about the maximum at position (b); consequently the surface temperature was 3300 K, 300 K higher than at (a). The corresponding variation of the band head intensities versus the distance from the surface (z direction) are plotted in Fig. 3. Near the surface ($0 \leq z \leq 1$ mm), the emission related to position (b) was more intense than the emission related to position (a) because the density of C_2 was higher in a vaporization plume from a graphite surface at 3300 K than from a surface at 3000 K and the solar irradiation was similar (Tables 1 and 2). But, for z longer than 1 mm ($z > 1$ mm) the reverse situation was observed even if the carbon species density was probably larger at (b) than at (a) as shown in Table 2. This result is again in agreement with our hypothesis.

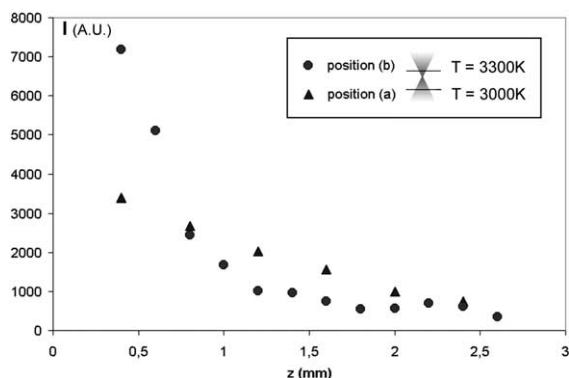


Fig. 3. Intensity of the C_2 band head as a function of the distance from the target surface at positions (a) and (b) – see Fig. 1 – pressure 70 hPa, argon flow rate 0.2 m³/h.

At position (b) carbon vapors were irradiated by decreasing solar irradiation for $z > 1$ mm. On the contrary, at position (a), increasing values of z corresponded to increasing values of the solar irradiation. Consequently, the emission was more intense in the latter case than in the former even if the C_2 density was smaller. Since the concentration of carbon species decreased with z in the mass transfer boundary layer, the C_2 emission vanished far from the graphite surface ($z \geq 2.5$ mm).

In addition, Table 2, Eqs. (1) and (2) permit to calculate the emission ratio (R) between position (a) and position (b) for a pure thermal process (R_T) and pure fluorescence (R_F). It comes:

- Thermal emission: $R_T = 4.4$;
- Fluorescence: $R_F = 2.8$;
- Measurement: $R = 2.2$.

Fluorescence-dominated C_2 emission is again supported by this comparison.

4. Discussion

From previous results we can eliminate all mechanisms leading to the formation of C_2 molecule excited states via dissociative or recombination processes. Otherwise, we must have measured the same emission intensity, at given temperature and pressure whatever the configuration. The Swan band emission from our system can originate from direct excitation of C_2 molecules by thermal agitation and photons absorption. Obviously both mechanisms happen at the same time but we claim that the latter is dominant.

First, slow diffusion-controlled vaporization of graphite occurs during our experiments with a mass transfer diffusion layer of about a 3 mm thickness ($P = 70$ hPa) [14]. Under these conditions vapor pressure and composition can be predicted by thermodynamics [20]. JANAF data [21] gives C_3 , C and C_2 as dominant species in the vapor at equilibrium in the temperature range 3000–3500 K. But C_2 formation is kinetically more favourable near 3000 K as shown in [22]. Moreover, Ebbesen et al. [23] argue that C_{60} is probably formed from atomic carbon (which is in equilibrium with C_2 and C_3 as discussed previously). On the contrary, pulse-laser ablation method gives rise

to a large amount of clusters and excited C_2 can be ejected from fragmented fullerenes. But, in these processes the laser intensity is about 120 MW/cm^2 [8,12,13]. With such high light intensity the C_{60} photo fragmentation, which requires more than 13 eV [9,13], can be achieved in the visible range of radiation, by multi-photon absorption process [13]. In our experiments the intensity of the solar concentrated beam is five orders of magnitude less and, consequently, a multi-photon absorption is an improbable process. In addition, due to the spectral distribution of the solar radiation and the optical properties of the concentrating system (UV absorption by glass), the energy of the available photons ranges practically from 2 to 3.5 eV and they are then unable to dissociate any carbon species. All these points support our assumption about the vapour composition dominated by carbon atom and small carbon molecules near the target.

Second, looking at the spectral distribution of solar energy at the ground level C_2 excitation is evidenced by the maximum intensity of solar energy in the wavelength range $0.5\text{--}0.6 \mu\text{m}$. This means that the maximum of irradiance is available from the sun in a broad spectral range of radiations able to excite simultaneously from the ground level all the rotational levels of the $C_2 \text{ d}^3\Pi_g$ state by single photon absorption processes.

Finally, we have derived carbon vapor temperature from Swan band emission data using a simplified method described in [16]. Typical results are shown in Fig. 4. Experimental data are compared with numerical simulation [14]. A satisfactory agreement is observed. Moreover, extrapolated gas temperatures at $z = 0$ and measured target temperature are also in agreement: the pyrometer measured a surface temperature of 3300 K. These data support the assumption of local thermodynamic equilibrium in the boundary layer. One can observe that there is a slight difference between the gas temperature listed in Table 2 (position (b), $T_g = 2950 \text{ K}$) and the gas temperature shown in Fig. 4 ($T_g = 3100 \text{ K}$) for the same target temperature (3300 K) and the same measurement position (0.5 mm above the surface). This 150 K-temperature difference illustrates the

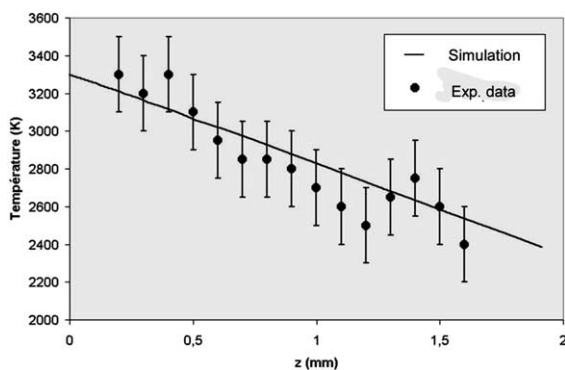


Fig. 4. Temperature distribution in the vaporization boundary layer obtained from C_2 emission (position b). Straight line: numerical simulation from [14]. Experimental conditions: Argon, 70 hPa, $0.4 \text{ m}^3/\text{h}$, and surface temperature: 3300 K.

measurement uncertainty because these data are related to two different sets of experiments. We estimate the uncertainty to be $\pm 200 \text{ K}$ and $\pm 0.05 \text{ mm}$ for the temperature and the measurement position respectively. The previous difference is consistent with these uncertainty ranges and it does not modify the conclusion obtained from Table 2.

5. Conclusion

Similarly to LIF we demonstrate the occurrence of SIF of C_2 in a high concentration solar system (concentration ratio of about 16000). This phenomenon is described for the first time and can be used for diagnostic. Works are in progress to define more precisely the condition of appearance of SIF and its possible influence on reaction processes.

References

- [1] H.W. Kroto, J.R. Heath, S.L. O'Brien, R.F. Curl, R.E. Smalley, *Nature* 318 (1985) 162.
- [2] W. Krätschmer, L.D. Lamb, K. Fostiropoulos, D.R. Huffman, *Nature* 347 (1990) 354.
- [3] L.P.F. Chibante, A. Thess, J.M. Alford, M.D. Diener, R.E. Smalley, *J. Phys. Chem.* 97 (1993) 8696.
- [4] C.L. Fields, J.R. Pitts, M.J. Hale, C.C. Bingham, A. Lewan Dowski, D.E. King, *J. Phys. Chem.* 97 (1993) 8701.

- [5] D. Laplace, P. Bernier, L. Barbedette, J.A. Lambert, G. Flamant, M. Lebrun, A. Brunelle, S. et Della-Negra, C.R. Acad. Sci. Paris 318 (Série II) (1994) 733.
- [6] T. Guillard, G. Flamant, J.F. Robert, B. Rivoire, J. Giral, D. Laplace, ASME J. Sol. Energy Eng. 124 (2002) 22.
- [7] T. Guillard, S. Cetout, G. Flamant, D. Laplace, J. Mater. Sci. 35 (2000) 419;
L. Alvarez, T. Guillard, J.L. Sauvajol, G. Flamant, D. Laplace, Chem. Phys. Lett. 342 (2001) 7.
- [8] M. Anselment, R.S. Smith, E. Daykin, L.F. Dimauro, Chem. Phys. Lett. 134 (5) (1987) 444.
- [9] O'S.L. Brien, J.R. Heath, R.F. Curl, R.E. Smalley, J. Chem. Phys. 88 (1988) 2809.
- [10] E.A. Rohlfing, J. Chem. Phys. 89 (10) (1988) 6103.
- [11] H. Lange, K. Saidane, M. Razafinimanana, A. Gleizes, J. Phys. D.: Appl. Phys. 32 (1999) 1024.
- [12] S. Arepelli, P. Nikolaev, W. Holmes, C.D. Scott, Appl. Phys. A 70 (2000) 125.
- [13] S. Arepelli, C.D. Scott, P. Nikolaev, R.R. Smalley, Chem. Phys. Lett. 320 (2000) 26.
- [14] T. Guillard, G. Flamant, D. Laplace, ASME J. Sol. Energy Eng. 123 (2001) 153.
- [15] G. Neuer, Int. J. Thermophys. 15 (1) (1995) 257.
- [16] S. Bousrih, E. Ershov-Pavlov, S. Megy, J.M. Baronnet, Plasma Chem. Plasma Process. 15 (2) (1995) 333.
- [17] A.C. Eckbreth, Laser Diagnostics for Combustion Temperature and Species, Gordon and Breach Publishers, London, 1996.
- [18] P.H. Paul, J. Quant. Spectrosc. Radiat. Transfer 51 (3) (1994) 511.
- [19] P.H. Paul, J.A. Gray, J.L. Durant Jr., AIAA J. 32 (8) (1994) 1670.
- [20] J.H. Lundell, R.R. Dickey, in: AIAA 14th Aerospace Sciences Meeting, Washington DC, 26–28 January 1976, paper 76–166.
- [21] J. Tables, J. Phys. Chem. Ref. Data (1985) 14.
- [22] J.A. Dolton, H.E. Goldstein, R.E. Maurer, AIAA J. 68 (1968) 754.
- [23] T.W. Ebbesen, J. Tabuchi, K. Tanigaki, Chem. Phys. Lett. 191 (3,4) (1992) 336.